1   **Upper Ocean Dynamics Select for *Synechococcus* Light Color Generalists**

2

3   **R. Lovindeer[1]†, L. J. Ustick[2], F. Primeau[1], A. C. Martiny[1,2], and K. R. M Mackey[1,2]†**

4

5   [1]University of California, Irvine, Department of Earth System Science Department.

6   [2]University of California, Irvine, Department of Ecology & Evolutionary Biology.

7

8   †Corresponding authors: Raisha Lovindeer (raisha.lovindeer@uci.edu), Katherine Mackey
9   (kmackey@uci.edu)

10

11   **Key Points:**

12   - Deep mixing, upwelling zones, and surface ocean gradients are important niches for
13   chromatic acclimating marine cyanobacteria.

14   - A high proportion of blue/green acclimaters at ocean fronts motivates future work on the
15   internal spectral variability of these regions.
16

17   **Abstract**

18   The ocean has many underwater light niches, but the selection pressure for chromatic acclimaters
19   (generalists) compared to blue or green-specialists is not well understood. Here, we tested the
20   hypothesis that changes in ocean spectra brought about by mixing on the order of days
21   preferentially selects for generalists within a *Synechococcus* population. We investigated ocean
22   conditions that led to high proportions of *Synechococcus* generalists versus specialists in a model
23   ocean column, and compared simulations with *in situ* metagenomic and physical oceanographic
24   data from major Bio-GO-SHIP cruises, supplemented with GEOTRACES and TARA Oceans, as
25   well as the GOOS Argo Program and sea surface height from AVISO. We found that greater
26   mixed layer depths selected for generalists in simulated *Synechococcus* populations, but
27   explained only 14% of the partitioning between strategies in situ. Rather, variability due to
28   upwelling and ocean fronts had larger effects, explaining ~40% of the partitioning between
29   *Synechococcus* generalists and specialists in the ocean. Physical oceanographic drivers therefore
30   offer a significant selection pressure on marine *Synechococcus* light-harvesting strategies. Our
31   results motivate further study of the *in situ* light environments of upwelling zones and ocean
32   fronts, which are currently understudied as potential light-driven niche habitats.

33

34   **Plain Language Summary**

35   The variety of pigments used by cyanobacteria to capture light for photosynthesis increases the
36   colors of light available for use in the ocean. One genus of cyanobacteria, *Synechococcus*, can
37   change color to absorb either blue or green light (generalists), adding to the variety of light-
38   harvesting strategies. Though the reason for this color change is believed to be fluctuations in the
39   underwater blue/green light field, this has not been tested directly. Using a mathematical model
40   of the ocean column, we find the highest percentages of generalists in the *Synechococcus*
41   population in deep ocean mixed layers. Comparison of model results to actual distributions of
42   generalists indicate that deep mixing plays a smaller role than our model suggested, and that
43   upwelling zones, where water is vertically moved to the surface, and ocean fronts, where major
44   ocean currents meet, are also important habitats for higher percentages of *Synechococcus*
45   generalists in the ocean.

46

47   **1. Introduction**

48   The terms *generalist* and *specialist* in ecology refer to organisms with differences in
49   tolerance or preference for food or habitat—generalists having weaker preferences and wider
50   tolerances. Examples are abundant in the literature and range from generalist bird species able to
51   adapt to disturbed environments (Viol et al., 2012) to the broad feeding habits of fish in Arctic
52   lakes (Laske et al., 2018). Among photosynthetic organisms in aquatic environments, feeding
53   and habitat preferences translate into nutrient and light-color acquisition, or light intensity,

54 temperature, and salinity tolerances. In cyanobacteria, preferential use of specific wavelengths of
55 light in aquatic ecosystems provides a colorful example of generalists—strains able to change
56 pigmentation to maximally absorb one wavelength over another (chromatic acclimation). In
57 lakes, rivers, estuaries, and oceans, light attenuates exponentially with depth, and partitions into
58 colors depending on the composition of the water. Aquatic cyanobacteria must be adapted to use
59 these available colors. Examples include high turbidity and increased colored dissolved organic
60 matter (CDOM) in lakes that result in mostly red light for photosynthesis, or blue light
61 dominating in clear, deep, open ocean water (Holtrop et al., 2020; Stomp et al., 2007). When the
62 color of underwater light changes in an ecosystem, generalists can undergo acclimation (Stomp
63 et al., 2004) whereas specialists may undergo succession (Luimstra et al., 2020; Stomp et al.,
64 2007).

65   To date, five types of chromatic acclimation strategies have been identified in coastal and
66 in-land waters (Sanfilippo et al., 2019). All are performed by cyanobacteria containing
67 phycobiliprotein light-harvesting pigments, though at least one strategy involves removal of
68 phycobilins in favor of chlorophyll-*d* (CA5). Strategies may include changes in the relative ratio
69 of phycobiliproteins (such as occurs in red and green light in CA2 and CA3), and rearrangement
70 of the phycobilisome core and attached chlorophylls (as in red & far/red light in CA6/FarLiP).
71 Blue/green chromatic acclimation (CA4, Palenik, 2001) is unique in that it is the only
72 acclimation type currently known to exist in the open ocean, is performed exclusively by
73 phycoerythrin-containing marine *Synechococcus*, and involves changes in the relative ratio of
74 chromophores attached to phycoerythrin, rather than a change in the ratio of the
75 phycobiliproteins themselves.

76   All *Synechococcus* CA4 generalists have phycobilisomes (light-harvesting structures that
77 house the phycobiliproteins) that contain phycocyanin and two types of phycoerythrin, PEI and
78 PEII, and are within the group of *Synechococcus* distinguishable by the presence of
79 chromophores phycoerythrobilin (PEB) and phycourobilin (PUB). PEB maximally absorbs light
80 in the range of 545 nm (green) and PUB maximally absorbs in the range of 495 nm (blue-green,
81 or cyan). In specialist strains, the ratio of PUB to PEB is fixed. Strains with high PUB:PEB are
82 herein referred to as blue-specialists, and low PUB:PEB as green-specialists. For CA4
83 generalists, the PUB:PEB ratio is variable. This variable PUB:PEB is controlled by groups of
84 genes within a genetic island, with two known variants, CA4-A and CA4-B (Humily et al.,
85 2013). The combination of phycobiliproteins and chromophores result in the categorization of
86 *Synechococcus* into pigment types (PTs) denoted by numbers: PT1- PT3 for the added presence
87 of phycocyanin, PEI, and PEII, respectively (Six et al., 2007). PTs can be further classified into
88 smaller groupings. PT3, for example, is further divided based on relative chromophore ratios,
89 and is the only PT containing generalists. PT3a - 3d designate low, medium, high, and variable
90 ratios of PUB to PEB (PUB:PEB), and strains containing whole or partial CA4-A or CA4-B gene
91 islands are denoted with the suffix A or B. These groupings are continuously expanded and
92 updated to include slight variations on the general ones listed here (Humily et al., 2013; Xia et
93 al., 2018).

94   The ecological niches of marine *Synechococcus* are determined mainly by temperature,
95   and nutrient availability, but CA4 generalists exist across these ecological niches (Ahlgren et al.,
96   2020; Ahlgren & Rocap, 2012; Farrant et al., 2016). Additionally, CA4-A and CA4-B strains
97   correlate with different environmental conditions (Grébert et al., 2018) making the reason for
98   evolutionary selection of CA4 difficult to identify. Given that CA4 is a spectral acclimation trait,
99   we may expect physical factors that influence the underwater color to also influence the ratio of
100 CA4 generalists to specialists. Since acclimation takes 4-6 days to complete (Humily et al., 2013;
101 Sanfilippo et al., 2016), variations with smaller timescales, such as cloud cover or light caustics,
102 can be ignored as key selection features for generalists (Stomp et al., 2008). On the contrary,
103 wind-driven mixing can change the light field for cyanobacteria within the mixed layer, moving
104 strains from wide spectrum surface waters to narrow spectrum deep waters that last throughout a
105 season. Areas prone to phytoplankton blooms, with high chlorophyll absorption at 440 nm, or
106 coccolithophore peak reflectance at 490 nm (Moore et al., 2012), also lead to underwater spectral
107 shifts that could select for generalists. The hypothesis that generalists may outcompete specialists
108 in areas with deep vertical mixing and/or high productivity has not been tested directly, but is
109 substantiated by the presence of higher abundances of generalists in regions that fit these
110 descriptions, such as the Chilean upwelling zone (Grébert et al., 2018).

111 Here, we explored the hypothesis that variations in the blue-green light field triggered by
112 physical mixing or changes in surface absorption (specifically, blue absorption by chlorophyll-
113 dominated plankton) result in higher percentages of generalists in the *Synechococcus* population.
114 We first investigated the effects of the timing of blue-green color variation in a hypothetical
115 ocean water column (Stomp et al., 2007, 2008), where CA4 generalists and blue and green
116 specialists compete solely based on their different spectra of light absorption and light-harvesting
117 strategies. Blue-green variations produced in the model light field were forced by oscillating
118 between two light colors, with oscillation periods that varied to be faster, at the same rate, and
119 slower than the pace of acclimation. Then, more akin to open ocean conditions, we tested the
120 effect of various depths of the homogenous mixed layer, and concentrations of chlorophyll-
121 dominated phytoplankton in daylight spectra. We compared model results to *in situ* data on the
122 proportion of *Synechococcus* generalists in metagenomic datasets collated from seven global
123 ocean cruises as part of the biological initiative of the Global Ocean Ship-based Hydrographic
124 Investigations Program (Bio-GO-SHIP), supplemented with four cruises from GEOTRACES,
125 and over 150 stations from TARA Oceans. Our focus on the partitioning of the *Synechococcus*
126 population allowed us to determine the specific drivers of high percentages of generalists relative
127 to specialists in the *Synechococcus* population.
128

2. Materials and Methods

2.1 Competition model

We simulated the time evolution of growth of *Synechococcus* PT3a (low PUB:PEB), PT3c (high PUB:PEB), and PT3d (variable PUB:PEB) strains (cells/m3) acclimating to blue and green light. This built on a previous study (Stomp et al., 2008) where three cyanobacteria populations competed for light based on the available light spectrum, using model equations for two fixed phenotypes and one flexible phenotype in red or green light as for CA3 strains. Each population was distinguished by their specific absorption spectrum as displayed in Fig. 1. All strains had equal maximum growth rates, p_{max}, photosynthetic efficiencies, φ, and loss rates, L (Table S1). Light penetration through the model followed exponential decay with available light at each depth layer influenced by absorption by seawater as well as the cyanobacteria populations. In our version of the model, the depth of the water column was variable, and additional absorption by chlorophyll and coccolithophores were added as options in addition to the absorption by seawater.

The model solution yielded the relative abundance of the three cyanobacteria pigment types integrated across the one-dimensional layer. Equilibrium was reached when light-limited growth was equal to loss. The model variables explored for their impact on the *Synechococcus* competing populations were the depth of the model layer, z_m; the incoming light spectra (whether blue/green/cyan and timing of oscillations, or the spectrum of daylight); and concentrations of chlorophyll or coccolithophores in the ambient water that affect light absorption by the competing strains. Descriptions of the model equations required to reproduce the results are provided in Supplemental Text S1, and model code (in MATLAB version 9.7.0, R2019b, MathWorks Inc.) is publicly available (Lovindeer, 2021).

2.1.1 Model environment & mixed layer depth

The model environment consisted of a one-dimensional aqueous layer of thickness, z_m, that was considered homogenous except for light penetration, which followed exponential decay by Beer-Lambert's law with depth. These conditions are similar to the dynamics of a well-mixed layer in the ocean, and z_m was considered synonymous with the mixed layer depth. The decay of light through the layer to z_m was calculated per wavelength at discrete depth intervals (Eqn. S3) and final results integrated from 0 to z_m. Simulations were made with various magnitudes of z_m, from 1 to 150 meters.

Light absorption with depth and wavelength were functions of the absorption spectrum of seawater (Buiteveld et al., 1994); absorption spectrum of each *Synechococcus* strain (Fig. 1); and absorption spectra of added ocean water constituents (chlorophyll and coccolithophores), concentrations of which were prescribed before each simulation (see 1.3 below). Each *Synechococcus* strain within the model was treated as a continuous tracer with increased light absorption over time and scattering properties ignored. Growth stagnated, and equilibrium was

166 reached, when light penetrating the aqueous layer limited growth to be equal to the prescribed
167 loss rate (Eqn. S6).

168   No parameters for mixing or turbulence were included. Variability between light colors
169 that may occur during mixing were externally forced by oscillating input light colors in the blue-
170 green region of the spectrum (see 2.1.2 below). The emission spectrum of daylight was used for
171 input light in all other simulations (2.1.3).

172   2.1.2   Time of oscillating light color

173   To simulate variability in light color that may occur in surface waters, oscillation between
174 blue, green, and cyan light spectra were used. Oscillations periods varied in timescale from faster
175 than acclimation times (< 1 day), at the same rate of acclimation (3 – 6 days) to beyond
176 acclimation time (> 10 days). Oscillations were created using a sine function, F, as a switch
177 between light colors (e.g. F > 0 blue, F < 0 green, Eqn. S8) with oscillation periods controlled by
178 a constant that resulted in five periods of 0.6, 3, 6, 11, and 31 days.

179   Incoming spectra for light colors (Fig. S1) were acquired from the emission spectra of
180 light emitting diodes (LEDs) in blue (PARsource), green (Illuminati), and cyan (Cyril
181 McCormick, University of California, Irvine), measured using an LI-180 spectrometer (LI-
182 COR). Blue LEDs had peak emission at 440 nm with shoulders ±30 nm consistent with the blue
183 light used to discover and subsequently document CA4 throughout the literature (Palenik, 2001;
184 Everroad et al., 2006; Six et al., 2007; Humily et al., 2013; Sanfilippo et al., 2016; Mahmoud et
185 al., 2017). Green LEDs had peak emission at 520 nm with shoulders ±40 nm. A cyan LED was
186 included to overlap the peak at 495 nm, but was not available commercially and was built from
187 diodes mounted to a copper board with heat sink. The resulting spectrum had higher emission at
188 495 nm but wide emission (430 – 620 nm). For comparison to a narrow emission band of cyan
189 light with peak at 495 nm, we created a spectrum in the model by mathematically shifting the
190 measured spectrum for the blue LED, with peak at 440 nm, to 495 nm.

191   Simulations with LED lights only included absorption from seawater and the competing
192 strains, with absorption by chlorophyll-a and coccolithophores set to 0.

193
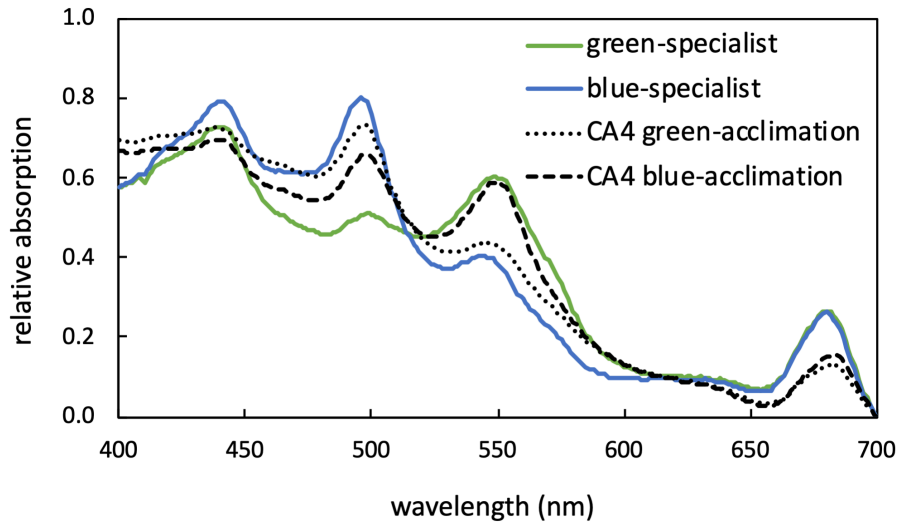
194

195 **Figure. 1**: Relative absorption spectra measured for *Synechococcus* strains WH8102 (blue-
196 specialist), WH7803 (green-specialist), and WH8020 fully acclimated to green light (CA4 green-
197 acclimation) and to blue light (CA4 blue-acclimation). Absorption spectra have been normalized
198 to zero absorption at 700 nm.

199

200   2.1.3   Constant daylight with chlorophyll absorption

201   Simulations in constant daylight used the above-water spectrum (μW cm^{-2} nm^{-1})
202 measured from 400 – 700 nm by an optical profiler deployed at the surface in "buoy mode" on a
203 TARA Mediterranean cruise in sunny conditions at 2pm on 26 Aug 2014 from 43.57 N, 7.33 W
204 (seabass.gsfc.nasa.gov/experiment/Tara_Mediterranean). Units were converted to μmol photons
205 m^{-2} s^{-1} nm^{-1} using a conversion factor from W m^{-2} to photons of 4.57 (Sager & McFarlane, 1997).
206 The resulting spectra is displayed in Fig. S1.

207   Chlorophyll-dominated phytoplankton were modeled using the specific absorption
208 spectrum of chlorophyll-*a*, which changed as a function of chlorophyll concentration(Bricaud et
209 al., 1995). Absorption of chlorophyll in the water column at each wavelength (m^{-1}) was
210 calculated by multiplying the specific absorption spectrum (m^2 mg^{-1}, Fig. S2) by the model's
211 prescribed chlorophyll concentration, which ranged from 0 – 20 mg m^{-3}. Absorption by
212 coccolithophores was calculated similarly, using the specific absorption spectrum of *Emiliania*
213 *huxleyi* (Sadeghi et al., 2012) (m^2 mg^{-1}, Fig. S2) and concentrations from 0 – 20 mg m^{-3}.

214   2.1.4 Model biology

215   Competing *Synechococcus* strains in the model were distinguishable by their specific
216 absorption spectra (Fig. 1). The rate of change for acclimation was determined by an acclimation
217 fraction, v, that was modified to increase PUB:PEB in ambient blue light and decrease PUB:PEB
218 in green light as described in Eqns. S1 – S2.

219   Growth of the strains over time was a function of their maximum growth rates, their
220   photosynthetic efficiencies, and the quanta of light absorbed per wavelength by each strain from
221   400 – 700 nm (Eqn. S6). Parameters for growth were acquired from monoculture laboratory
222   experiments with *Synechococcus* strains WH8102 (blue-specialist), WH7803 (green-specialist),
223   and CA4 acclimaters RS9916 and WH8020, in nutrient replete conditions under blue, green, and
224   white LED light (Table S1). The model was calibrated using input light emissions that matched
225   the continuous LED lights used in experiments. Maximum growth rates (0.7 day^{-1} in green light,
226    $p_{max,green}$, and 0.5 day^{-1} in blue light, $p_{max,blue}$), photosynthetic efficiency (2.4 x 10^6 cells
227   (μmol photons)$^{-1}$ in green light, φ_{green}, and 1.2 x 10^6 cells (μmol photons)$^{-1}$ in blue light, φ_{blue}),
228   and a prescribed loss rate of 0.005 hr^{-1} (L) were kept constant for all strains within the model.
229   This ensured that differences in growth were only attributable to differences in absorption
230   spectra. The concentration of each strain integrated across z_m was calculated per unit time.
231   Abundances at model equilibrium were converted to percentages of the final population at
232   equilibrium for comparison across model simulations.

233   2.2 *In* situ data

234   Available cruise data from campaigns in the Atlantic, Pacific and Indian Oceans from
235   2009 to 2018 were collated and used in this study. This included 11 cruise transects–Bio-GO-
236   SHIP AE1319, NH1418, BV46, AMT28, IO9, IO7, P18, (Larkin et al., 2021) GEOTRACES
237   GA02, GA03, GA10 & GP13 (Biller et al., 2018; Schlitzer et al., 2018)–and 153 stations from
238   TARA Oceans (Picheral et al., 2014; Sunagawa et al., 2015). Correlation analyses were
239   performed on the proportion of generalists in the *Synechococcus* population. Analyses were
240   performed in MATLAB.

241   2.2.1 Metagenomic processing of cruise data

242   Raw metagenomic reads were quality controlled, and adapter sequences trimmed using
243   Trimmomatic v0.35 (Bolger et al., 2014). Trimmed reads were recruited to a reference dataset of
244   115 genomes with representatives of each ecotype of *Synechococcus*, *Prochlorococcus,* and
245   *Pelagibacter* as well as a *Roseobacter* reference to help reduce false recruitment of closely
246   related reads. Bowtie2 v2.2.7 (Langmead & Salzberg, 2012) was used for read recruitment with
247   the following flags: --no-unal --local -D 15 -R 2 -L 15 -N 1 --gbar 1 --mp 3. Resulting SAM files
248   were sorted and indexed into BAM files using samtools v1.3 (Li et al., 2009). Recruited reads
249   were then profiled using Anvi'o v5 (Eren et al., 2015). Genes were identified by aligning and
250   clustering all open reading frames in the reference dataset using NCBI BLAST (Altschul et al.,
251   1990) and MCL (van Dongen & Abreu-Goodger, 2012) through the Anvi'o pangenomic
252   workflow (Delmont & Eren, 2018). The clusters were curated selecting genes of interest (Table
253   S2) and coverages were calculated using MATLAB scripts (version 9.5.0, R2018b; Ustick,
254   2021).

255   2.2.2 Estimation of pigment type abundances

256   The relative abundance of generalists (PTs 3d & 3e) and specialists (PTs 3a, 3b, 3c, & 3f)
257   were calculated using the coverage of the genes *mpeAB* and *mpeW* matched to PTs (Grébert et
258   al., 2018)(Table S2). Total PT abundance was estimated by normalizing coverages to raw read
259   pair counts per sample. Samples with less than 5x total *mpeAB* coverage were removed from the
260   analysis.

261   2.2.3 Assignment of pigment type for unknown genomes

262   To identify the pigment type of uncharacterized reference genomes, a phylogeny of the
263   *mpeAB* genes was created. The sequences were aligned using Mega7 (Kumar et al., 2016) and
264   Muscle (Edgar, 2004). Maximum likelihood fits of 24 different nucleotide substitution models
265   were estimated using MEGA7, and GTR+Gamma was selected due to low Bayesian Information
266   Criterion and Akaike Information Criterion values. A phylogenetic tree was generated using
267   raxml (Stamatakis, 2014) with the following arguments -T 6 -f a -x 123 -p 123 -N 1000 -m
268   GTRGAMMA -O. PT3 variants were assigned based on *mpeAB* sequence variation and also the
269   presence-absence of *mpeW* and *mpeZ* in the reference genome (Fig. S3). Resulting tree, bootstrap
270   values, and assignments were visualized using iTOL (Letunic & Bork, 2007).

271   2.3 Mixed layer depth (MLD) and temperature from cruise data

272   Data from cruise CTD profiles were downloaded for each cruise from publicly available
273   repositories for GO-SHIP from https://cchdo.ucsd.edu accessed 13-Feb-2020, GEOTRACES
274   intermediate data product 2017 version 1 from http://www.bodc.ac.uk/geotraces/data/idp2017
275   accessed 02-Oct-2020 (Schlitzer et al., 2018), and TARA Oceans stations $001 - 210$ from
276   http://oceans.taraexpeditions.org accessed 28-Oct-2020 (Picheral et al., 2014).
277   A range of methods exist in the literature for calculating mixed layer depth (de Boyer
278   Montégut, 2004; Holte & Talley, 2009) and MLD calculations were compared across these
279   methods using the methodology described in (Holte & Talley, 2009). A dataset for calculating
280   seawater density parameters used for MLD calculations (seawater_ver3_3.1.zip downloaded on
281   02-Dec-2020) was provided by the Commonwealth Scientific and Industrial Research
282   Organisation (CSIRO) through a Creative Commons Attribution 4.0 International Licence. The
283   threshold method (de Boyer Montégut, 2004) with a temperature threshold of 0.2°C from a
284   surface reference of 10 m was used for this study, as this method aligned best with visually
285   inspected profiles from cruise CTD casts. Match-ups between calculated MLDs from CTD
286   profiles and the proportion of *Synechococcus* PTs yielded 629 points for correlation analyses.
287   The average temperature of the mixed layer was calculated by averaging all temperature values
288   between the 10 m reference depth and the mixed layer depth. Temperature values were reported
289   in the text ± one standard deviation.

290   2.3 Mixed layer depth monthly climatology

291   Data on monthly mixed layer depth climatology (Holte et al., 2017) from the Global
292   Ocean Observing System Argo Program was downloaded in MATLAB format on 17-Sep-2020
293   from a public repository at the University of California, San Diego (http://mixedlayer.ucsd.edu).
294   The dataset was used to create the climatological means from January 2000 to December 2019.
295   Monthly mean mixed layer depth was retrieved for the month and grid sampling location of each
296   *Synechococcus* genetic data point. A total of 605 co-located data points were used for analyses.

297   2.4 Sea Surface Height climatology and gradients

298   Monthly, binned, 1 degree gridded level 4 absolute dynamic topography / sea surface
299   height above the geoid (SSH, m) from October 1992 to December 2010 was retrieved on 29-
300   Dec-2020 from the Physical Oceanography Distributed Active Archive Center (PO.DAAC) at
301   NASA's Jet Propulsion Lab . The SSH dataset was derived from measurements by several
302   satellites (Envisat, TOPEX/Poseidon, Jason-1 and OSTM/Jason-2) and was provided by
303   Archiving, Validation, and Interpretation of Satellite Oceanographic Data (AVISO, 2011).
304   Values were averaged by month to obtain monthly climatology of SSH from 1992 – 2010. Co-
305   located values matching the month of sampling of each genetic data point was retrieved from the
306   dataset and yielded 569 matched values. SSH gradients were calculated using absolute
307   differences in SSH between nearest one-degree grid cells.

308   2.5 Statistical analyses

309   All statistical analyses were performed in MATLAB. Linear regression analyses were
310   conducted for results of the model simulations and *in-situ* data correlations. Correlation analyses
311   for *in situ* data were conducted between all physical oceanographic parameters and the percent of
312   generalists in the *Synechococcus* population calculated as the combined read abundances of
313   PT3d over total *mpeAB* reads. Regression coefficients (R^2), p-values (p), and the number of
314   samples for each analysis (n) are reported in the text or figure legends.

315

316   **3. Results**

317   *Conceptual model*
318   We modified a one-dimensional model of competition between cyanobacteria strains with
319   different light-harvesting strategies and absorption spectra, based on equations in (Stomp et al.,
320   2008), and tested the light-dependent factors driving the abundance of chromatic acclimating
321   generalists in the population. The model simulated the time evolution of growth (cells/m^3) of
322   three strain populations that represented *Synechococcus* pigment types—a green-specialist PT3a,
323   a blue-specialist PT3c, and a generalist PT3d. We tested the effect of three variables on the
324   proportion of generalists in the resulting population at equilibrium. These were: 1) the timing of
325   oscillation between two light colors (blue/green, blue/cyan, cyan/green) which varied from faster

326 than acclimation (0.6 days), within the same pace of acclimation (3 – 6 days) and slower than
327 acclimation (11 – 31 days); 2) depth of z_m (the homogenous layer); and 3) increasing
328 chlorophyll-a and coccolithophore absorption in daylight.
329   The percentage of generalists in the *Synechococcus* population was determined primarily
330 by the depth of the homogenous layer ($R^2 = 0.73$, p < 0.001, n = 77; Fig. 2). For all simulations,
331 whether in LED light colors or in daylight, the percentage of generalists increased as z_m
332 increased (Fig. 2). Panels a – c in Figure 2 display an example at 3-day oscillation period with
333 generalists dominating at z_m > 10 m. Similarly, in daylight (panels d – f) at constant
334 concentration of 0 and 15 mg m^{-3} chlorophyll-*a*/coccolithophore absorption, generalists
335 consistently dominated at deeper z_m, while green-specialists dominated at shallower z_m.
336 Absorption by chlorophyll-*a* and coccolithophores favored the green-specialist and increased the
337 depth at which generalists dominated the population. For example, generalists were 100% of the
338 population at 80 m z_m in clear water (panel d) and 140 and 100 m z_m with 15 mg m^{-3} added
339 chlorophyll-*a* and coccolithophore absorption, respectively (panels e and f).
340   We note that the acclimation fraction, v, that controls the extent of acclimation and
341 ranges from fully acclimated to low PUB:PEB at $v = 0$ to fully acclimated to high PUB:PEB at
342 $v = 1$ remained at 0.4 in clear water simulations in daylight with z_m > , indicating an
343 intermediate PUB:PEB acclimation range was maintained by the generalist strain. These
344 simulations were the only ones for which v did not equilibriate to 0 or 1. Chromatic acclimaters
345 have been shown to maintain intermediate PUB:PEB ranges when illuminated with different
346 ratios of blue and green light (Sanfilippo et al., 2016), such that the acclimation response is not
347 binary.
348   Oscillation time between light colors had no effect on the percentage of generalists in the
349 population. An example of the results at 1m depth and varying oscillation times is displayed in
350 Fig. S4 panel a. The green-specialist dominated at 1 m z_m during blue/green, blue/cyan, and
351 cyan/green oscillations. That the green-specialist dominated during blue/cyan oscillations was
352 linked to the wide spectrum of the cyan LED used in the simulations. However, a much narrower
353 cyan spectrum with a distinct peak at 495 nm led to the blue specialist dominating (Fig. S4, panel
354 b). This indicates that the blue-specialist requires a narrow band of blue-shifted wavelengths
355 (between 440 – 495 nm) to dominate the population. A blue-dominance requirement for the blue-
356 specialist was reinforced in daylight simulations, where the green-specialist dominated in clear
357 water (0 mg m^{-3} added chlorophyll or coccolithophore absorption). The spectrum of daylight
358 used in our simulations had a blue region spanning 450 – 500 nm that diminished more rapidly
359 with depth in comparison to the green region (500 – 550 nm) once competing strains were
360 present (Fig. S5). When the green-specialist was removed from the simulation, the blue-
361 specialist dominated at 1 m z_m in daylight. Thus, the blue-specialist may only dominate in the
362 near absence of other strains, when the water column can maintain high ambient emission in the
363 blue region.
364

Legend: Generalist (dashed) — Green-specialist — Blue-specialist
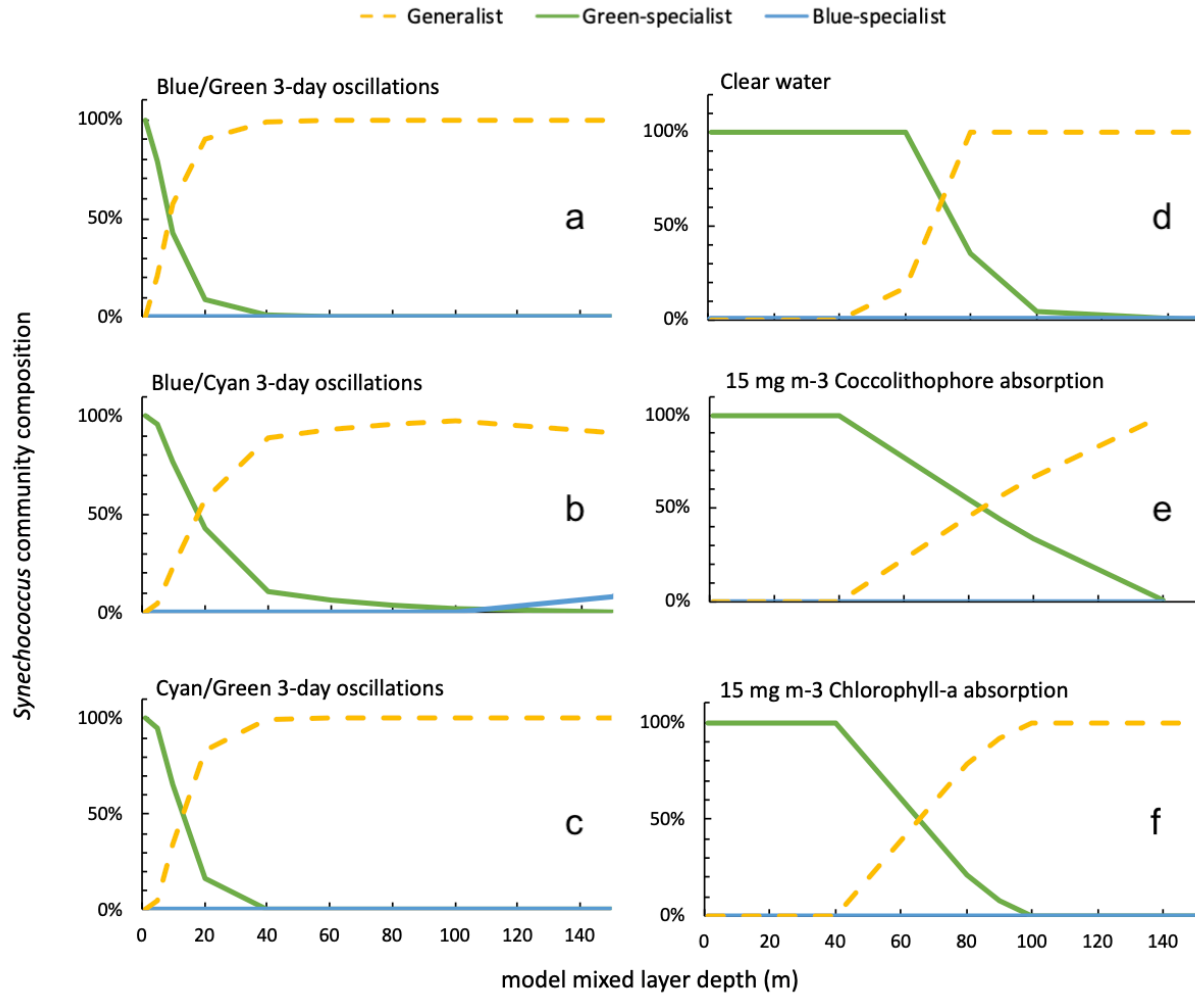
Figure. 2: Simulated population distribution at steady state equilibrium of *Synechococcus* generalist and specialists at various magnitudes of z_m. Panels **a - c** show results under continuous 3-day oscillation periods between two LED lights in the blue-green spectral region. Panels **d - f** show results under daylight with no additional pigment absorption (**d**) and absorption resulting from 15 mg m^{-3} added coccolithophores (**e**) and chlorophyll-*a* (**f**).

With generalists only dominating at larger z_m, the results of our simulations suggest that the depth of the mixed layer is the main driver of the partitioning between *Synechococcus* generalists and specialists. As the model is a conceptual exploration into deterministic changes in the light field, it does not account for other factors that affect the distribution of *Synechococcus* in the ocean, such as nutrients and temperature (Zwirglmaier et al., 2008; Kent et al., 2019; Ahlgren et al., 2020). Thus, model results are confined to describing the light-dependent driver of the partitioning of the *Synechococcus* population.

Generalists in situ

381   To test whether mixed layer depth strongly selected for generalists *Synechococcus* strains
382 in the open ocean, we examined metagenomic data from 11 cruise transects (7 Bio-GO-SHIP and
383 4 GEOTRACES) along with 153 stations from TARA Oceans, for which concurrent
384 conductivity, temperature and depth (CTD) profiles were available for mixed layer depth (MLD)
385 calculations. MLD was calculated using the method of (de Boyer Montégut, 2004) with a
386 temperature threshold of 0.2^{o}C from a surface reference of 10 m, which worked best for the
387 profiles in our dataset. The *Synechococcus* population was identified using the *mpeAB* gene
388 marker mapped to PTs (Grébert et al., 2018) and generalists were defined as the combination of
389 PTs 3dA+3dB.

390   From global ocean cruise metagenomic data, *Synechococcus* had the highest percentage
391 of generalists in high latitude regions above 30° north and south and within the Pacific equatorial
392 upwelling zone (Fig. 3a).

393
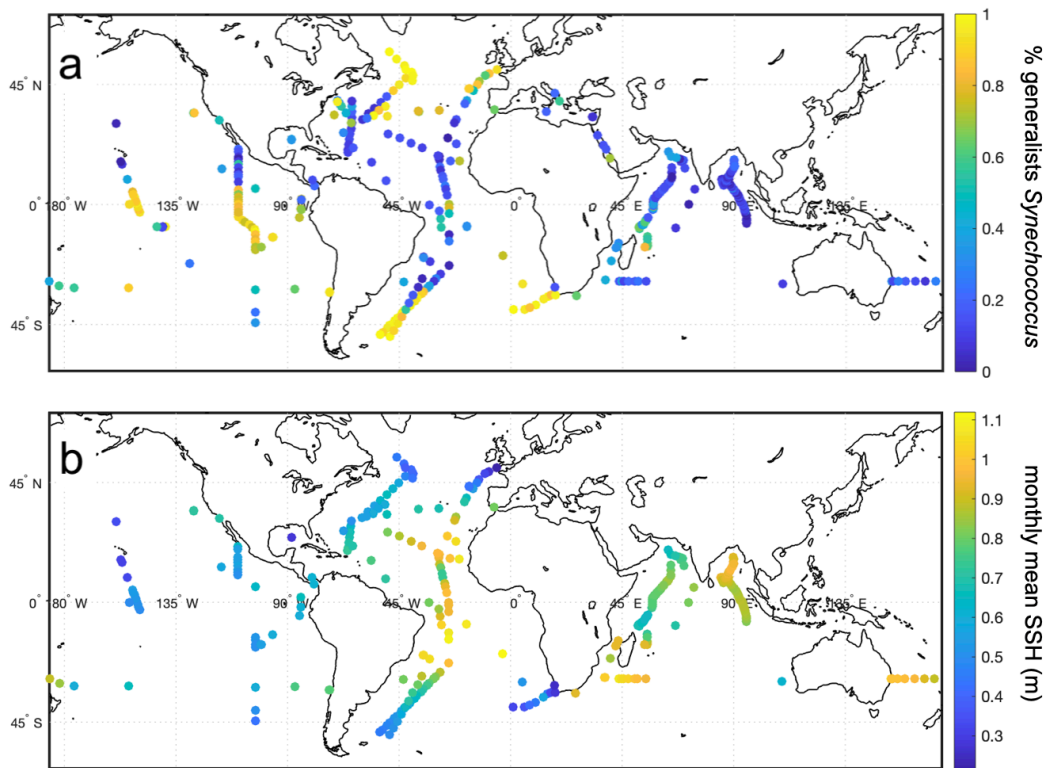
394
395 **Figure. 3**: Global patterns of *Synechococcus* light-harvesting strategies and co-located sea
396 surface height climatology. **a**) Percentage of *Synechococcus* CA4 acclimaters (pigment types
397 3dA+3dB) normalized to total *mpeAB* reads >5x total coverage from metagenomic datasets
398 between 2009-2018. **b**) Co-located monthly climatology of sea surface height (m) from 1992 -
399 2010 (569 points).

400

In contrast to the model simulations, MLD calculated from cruise data did not correlate strongly with *Synechococcus* light-harvesting strategies. The percentage of generalists had low correlations with MLD calculated from CTD profiles across the dataset ($R^2 = 0.04$, n = 629, Fig. 4a). However, it is possible that point sampling of a CTD profile at oceanic stations does not correlate well with the average MLD experienced at that station. For example, a mixed layer may shoal on a particularly warm day of sampling in a region with an average deeper MLD. High percentages of generalists along cruise tracks in similar areas but different sampling times (Fig. 3a) indicate possible adaptation to the mean state of ocean niche conditions. To account for a possible mismatch in timescale between point sampling and the average MLD that the strains may experience, we correlated the proportion of generalists with the climatological monthly mean MLD from *in-situ* data generated by National Oceanic & Atmospheric Administration's (NOAA) Global Ocean Monitoring & Observing autonomous Argo floats. CA4 strains had higher positive correlations with monthly MLD climatology ($R^2 = 0.14$, n = 605, Fig 4b) indicating that average MLD have a more significant role in the partitioning of *Synechococcus* light-harvesting strategies.
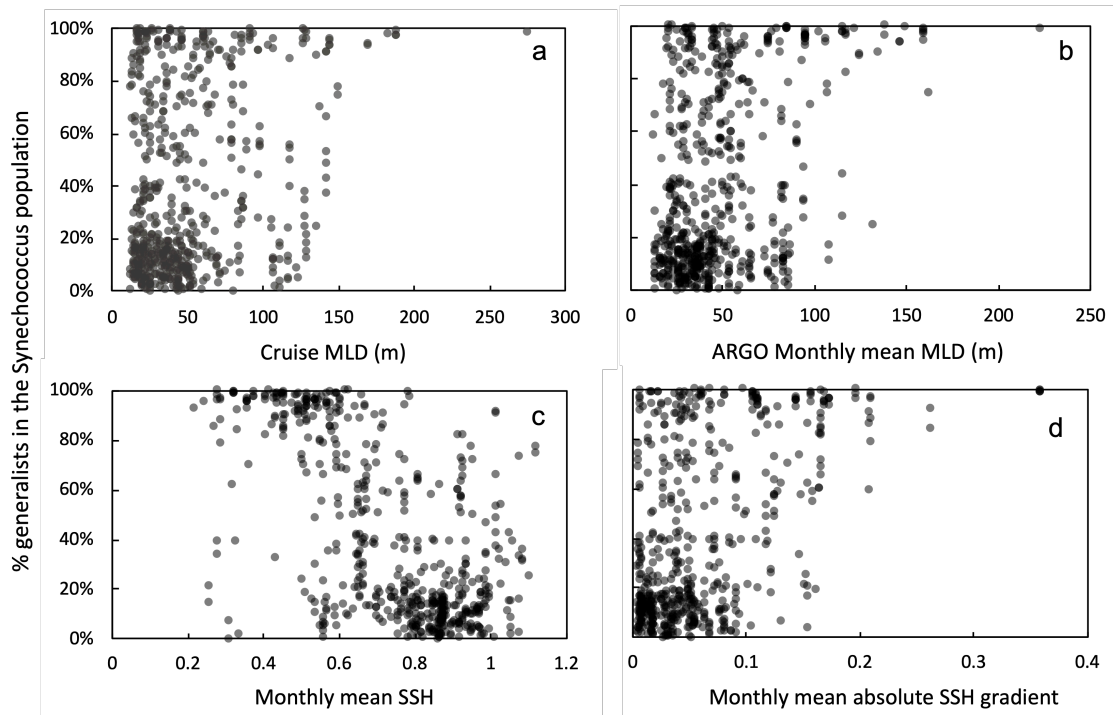

Figure. 4: Scatter plot of the percentage of *Synechococcus* CA4 acclimaters correlated with co-located physical oceanographic properties. **a**) Mixed layer depth (MLD, m) from cruise CTD data retrieved from the same cruises as *Synechococcus* metagenomic samples ($R^2 = 0.04$, n = 629). **b**) Monthly mean MLD climatology from ARGO float data from Jan 2000 to Dec 2019 ($R^2 = 0.14$, n = 605). **c**) Monthly SSH climatology (m) from Oct 1992 to Dec 2010 satellite data ($R^2 = 0.39$, p < 0.001, n = 569). d) SSH absolute gradient (m) ($R^2 = 0.23$, p < 0.001, n = 560).

425   Much higher correlations were evident with the mean temperature of the mixed layer
426 taken from cruise CTD data. Mixed layer average temperatures ranged from 9.6±0.1 °C to
427 31.2±0.2 °C. Generalists dominated at temperatures below 14°C and were significantly
428 anticorrelated with temperature across the dataset ($R^2 = 0.47$, $p < 0.01$, $n = 629$). The generalists
429 in our dataset were dominated by PT 3dA strains, found to be in high abundance in cold waters
430 (Grébert et al., 2018).

431   The distribution in Figure 3a indicates higher percentages of generalists in areas of major
432 ocean fronts, where cold and warm currents meet, which could provide significant energy for
433 upper ocean turbulence (D'Asaro et al., 2011) not tested within our model. We investigated this
434 relationship using the climatological mean absolute dynamic topography, or sea surface height
435 with respect to the geoid (SSH), as a remote sensing proxy for ocean fronts (Sun et al., 2011).
436 Using one-degree binned satellite data, we calculated gradients in SSH surface topography, as
437 higher gradients are indicative of oceanic frontal systems. CA4 strains positively correlated with
438 absolute SSH gradients ($R^2 = 0.23$, $p < 0.01$, $n = 560$, Fig 4c). Similar to correlations with
439 temperature, CA4 strains were highly correlated with low SSH ($R^2 = 0.39$, $p < 0.001$, $n = 569$,
440 Fig 4d).

441

4. Discussion

443   This study revealed that deep mixed layers, upwelling zones, and sea surface height
444 gradients, indicative of ocean fronts, are large-scale physical drivers of the partitioning between
445 *Synechococcus* light-harvesting generalists and specialists. Deep mixed layers in the model
446 environment with growing cyanobacteria strains reduced light availability in both blue and green
447 spectral regions over time (Fig. S5). The dominance of generalists with depth in the model could
448 reflect the benefit of their ability to manage an intermediate state in which there is equally strong
449 light absorption in both the blue and green spectral regions. Such was the case for the generalist
450 strain that maintained an intermediate PUB:PEB range (expressed as $v = 0.4$) in deep water. This
451 result indicates that in addition to environments for which generalists can fully acclimate to
452 either blue or green, a second, stable intermediate niche space exists for generalists, where light
453 can be available near equally in both 495 and 545 nm spectral regions. Such a stable intermediate
454 niche would only be applicable to phenotypic plasticity that is non-binary, as is the case for
455 chromatic acclimation.

456   A stable intermediate may also explain why light that varied faster than the acclimation
457 time had no effect on the dominance of the generalists. Equal absorption at both 495 and 545 nm
458 by the generalist was not evident during fast oscillation times in our model, but if the
459 environment changed too rapidly, strains may acclimate to the average of the changing
460 environment, which may be sensed as a static environment rather than a variable one. If that
461 static environment is not the two end member colors, but rather a combination, a non-binary
462 generalist may still be able to thrive. However, this idea is not supported by other non-binary

463 phenotypes for which timescales of variation have been shown to be important. Timescales faster
464 than the acclimation time modeled for the CA3 cyanobacteria strain *Pseudanabaena* CCY9509
465 did not favor the strain, and instead were too fast for the generalist to effectively outcompete
466 both green and red specialists (Stomp et al., 2008). Recent work (Walworth et al., 2020) has
467 shown that rapid fluctuations in physical environmental conditions that occur on timescales
468 shorter than 10 microbial cell generations select for generalists (what the authors call low g-
469 strategies), and prevent the evolution of specialists (high g-strategies), while stable environments
470 more quickly selected for specialists. Chromatic acclimation is completed within 6 microbial cell
471 generations (Everroad et al., 2006), and would benefit from such rapid fluctuations. Upwelling
472 zones can transport water vertically at a rate of 12 m day^{-1} and horizontally by 6 km day^{-1}
473 (Tilstone et al., 2000), and could be considered rapid fluctuations. For *Synechococcus* strains
474 with average nutrient replete growth rates of 0.7 day^{-1}, vertical transport from deeper than 50 m
475 would align with acclimation times for generalists, driving their dominance in these
476 environments. This is supported by other studies reporting high abundances of generalists in the
477 *Synechococcus* CRD1 and CRD2 clades that dominate the Costa Rica upwelling dome, as well
478 CA4 strains in the Benguela upwelling, and the equatorial Pacific upwelling regions observed in
479 our dataset (Grébert et al., 2018; Sohm et al., 2016).

480   For deep mixing in the open ocean, vertical movement and turbulence create variability
481 for each individual strain that was not able to be replicated in our model. Deep mixed layers also
482 introduce more limiting light environments if mixing goes deeper than the euphotic zone depth,
483 which varies spatially as a function of chlorophyll from less than 10 m to greater than 80 m (Lee
484 et al., 2007). These factors could explain the large disparity between modeled and *in-situ*
485 correlations of generalists with MLD. A useful expansion to the current model may include
486 vertical exchange of phytoplankton with the inclusion of mixed layer diffusivity to examine the
487 spread of strains throughout the layer and calculate their ambient spectra with time. As mixed
488 layer diffusivity changes with seasons (Cronin et al., 2015), annual variability in diffusivity as
489 well as depth of the mixed layer and euphotic zone could be modeled in tandem. This would
490 provide useful information about how the proportion of light-harvesting strategies within the
491 *Synechococcus* community changes throughout seasonal cycles, and may explain the
492 climatological mean observations presented here.

493   The stark gradient of light harvesting strategies across temperature and sea surface height
494 indicate an important role of currents in the partitioning of *Synechococcus* strains. Ocean fronts
495 can cause re-stratification of the upper surface water, decreasing the MLD (Taylor & Ferrari,
496 2011) on a timescale of days (Mahadevan et al., 2010) and forming an independent selection
497 pressure for generalists in shallower MLDs. Though many studies have focused on nutrient and
498 light interactions for phytoplankton production at ocean fronts (Lima, 2002; Mahadevan, 2016),
499 no studies have resolved the impact of turbulence on the spectrum of visible light with depth in
500 these regions. As nutrient-light interactions within ocean fronts trigger phytoplankton blooms
501 (Taylor & Ferrari, 2011), we might expect a compounding effect of ocean water and chlorophyll
502 absorption on variation in the blue-green spectral region in these areas. Future studies in this area

503 could expand the one-dimensional model explored here to include episodic exchange between
504 deep and shallow mixing depths and explore the time variability of mixing, turbulence, and
505 blooms that could more readily lead to the selection of generalists we observe in the ocean.
506 General studies of the picoplanktonic composition of ocean fronts are also lacking. Most studies
507 on phytoplankton at ocean fronts focus on the movement of nutrients and the resulting
508 chlorophyll-dominated blooms observable by satellite (for example d'Ovidio et al., 2010;
509 Mahadevan, 2016). There is less focus on the effect of turbulence on the underwater spectrum, or
510 the picoplanktonic community that can result from changes in that light spectrum, leaving this
511 potential niche of *Synechococcus* generalists critically understudied.

512   Horizontal advection by ocean currents has been shown to affect the distribution of
513 phytoplankton niches *in situ* (d'Ovidio et al., 2010), becoming conduits for transfer of plankton,
514 potentially outside their preferred niches. Though horizontal advection was not modeled in our
515 study, we expect that specialists that have been horizontally transferred beyond their tolerances
516 for light, nutrients or temperature would not readily survive, while generalists, with wider
517 tolerances, may continue to thrive during advection. As such, horizontal advection could provide
518 another physical oceanographic selection pressure for generalists that requires further study.

519   Together, physical ocean mixing contributes strongly to the partitioning of light-
520 harvesting strategies in the *Synechococcus* population. In addition to nutrient kinetics known to
521 trigger phytoplankton blooms, wavelength acclimation may play a significant role in ocean
522 frontal zones and upwelling areas. Thus, in addition to static ocean niches, dynamic ocean niches
523 seemingly impose their own selection pressure on the phytoplankton community structure,
524 selecting for flexible light color harvesting phenotypes.

525

526   5. Conclusions

527   Physical mixing of ocean water is a selection pressure for the generalist light-harvesting
528 strategy of chromatic acclimation in marine *Synechococcus*. High proportions of chromatic
529 acclimaters within the *Synechococcus* population were positively correlated with deep mixed
530 layers, low sea surface temperature, low sea surface height, and large sea surface height
531 gradients in areas of major ocean currents. Climatological means of these ocean variables were
532 yielded higher correlations, indicating a possible adaptation of acclimaters to the mean state of
533 mixing present in upwelling zones and ocean fronts. This study indicates that ocean niches with
534 large-scale vertical movement and surface turbulence offer a substantial selection pressure within
535 the phytoplankton, and helps to explain the wide diversity of photosynthetic pigment strategies
536 within marine *Synechococcus*, one of the most ubiquitous cyanobacteria in the ocean.

537

Conflict of Interest

The authors declare no conflicts of interest

Data availability

All datasets generated from this research are publicly available. Model code used to generate the light color competition simulations is available at https://doi.org/10.5281/ZENODO.4663350, with the resulting dataset at https://doi.org/10.7280/D16688. MATLAB scripts used to identify *Synechococcus* gene coverage is available at https://doi.org/10.5281/zenodo.4677447. The resulting *in situ* dataset of co-located *Synechococcus* pigment types and physical oceanographic parameters of mixed layer depth, mixed layer depth properties (temperature, salinity, and density) and climatology, sea surface height, and sea surface gradients is available at https://doi.org/10.7280/D1XQ2P.

569

570 **References**

571 Ahlgren, N. A., Belisle, B. S., & Lee, M. D. (2020). Genomic mosaicism underlies the adaptation of marine

572   *Synechococcus* ecotypes to distinct oceanic iron niches. *Environmental Microbiology*, *22*(5), 1801–1815.

573   https://doi.org/10.1111/1462-2920.14893

574 Ahlgren, N. A., & Rocap, G. (2012). Diversity and Distribution of Marine Synechococcus: Multiple Gene

575   Phylogenies for Consensus Classification and Development of qPCR Assays for Sensitive Measurement of

576   Clades in the Ocean. *Frontiers in Microbiology*, *3*. https://doi.org/10.3389/fmicb.2012.00213

577 Altschul, S. F., Gish, W., Miller, W., Myers, E. W., & Lipman, D. J. (1990). Basic local alignment search tool.

578   *Journal of Molecular Biology*, *215*(3), 403–410. https://doi.org/10.1016/S0022-2836(05)80360-2

579 AVISO. (2011). *AVISO Level 4 Absolute Dynamic Topography for Climate Model Comparison* [Data set]. NASA

580   Physical Oceanography DAAC. https://doi.org/10.5067/DYNTO-1D1M1

581 Biller, S. J., Berube, P. M., Dooley, K., Williams, M., Satinsky, B. M., Hackl, T., Hogle, S. L., Coe, A., Bergauer,

582   K., Bouman, H. A., Browning, T. J., Corte, D. D., Hassler, C., Hulston, D., Jacquot, J. E., Maas, E. W.,

583   Reinthaler, T., Sintes, E., Yokokawa, T., & Chisholm, S. W. (2018). Marine microbial metagenomes

584   sampled across space and time. *Scientific Data*, *5*(1), 1–7. https://doi.org/10.1038/sdata.2018.176

585 Bolger, A. M., Lohse, M., & Usadel, B. (2014). Trimmomatic: A flexible trimmer for Illumina sequence data.

586   *Bioinformatics*, *30*(15), 2114–2120. https://doi.org/10.1093/bioinformatics/btu170

587 Bricaud, A., Babin, M., Morel, A., & Claustre, H. (1995). Variability in the chlorophyll-specific absorption

588   coefficients of natural phytoplankton: Analysis and parameterization. *Journal of Geophysical Research*,

589   *100*(C7), 13321. https://doi.org/10.1029/95JC00463

590 Buiteveld, H., Hakvoort, J. H. M., & Donze, M. (1994). *Optical properties of pure water* (J. S. Jaffe, Ed.; pp. 174–

591   183). https://doi.org/10.1117/12.190060

592 Cronin, M. F., Pelland, N. A., Emerson, S. R., & Crawford, W. R. (2015). Estimating diffusivity from the mixed

593   layer heat and salt balances in the North Pacific. *Journal of Geophysical Research: Oceans*, *120*(11), 7346–

594   7362. https://doi.org/10.1002/2015JC011010

595 d'Ovidio, F., Monte, S. D., Alvain, S., Dandonneau, Y., & Lévy, M. (2010). Fluid dynamical niches of

596   phytoplankton types. *Proceedings of the National Academy of Sciences*, *107*(43), 18366–18370.

597   https://doi.org/10.1073/pnas.1004620107

598   D'Asaro, E., Lee, C., Rainville, L., Harcourt, R., & Thomas, L. (2011). Enhanced Turbulence and Energy

599   Dissipation at Ocean Fronts. *Science*, *332*(6027), 318–322. https://doi.org/10.1126/science.1201515

600   de Boyer Montégut, C. (2004). Mixed layer depth over the global ocean: An examination of profile data and a

601   profile-based climatology. *Journal of Geophysical Research*, *109*(C12), C12003.

602   https://doi.org/10.1029/2004JC002378

603   Delmont, T. O., & Eren, A. M. (2018). Linking pangenomes and metagenomes: The Prochlorococcus

604   metapangenome. *PeerJ*, *6*, e4320. https://doi.org/10.7717/peerj.4320

605   Edgar, R. C. (2004). MUSCLE: Multiple sequence alignment with high accuracy and high throughput. *Nucleic*

606   *Acids Research*, *32*(5), 1792–1797. https://doi.org/10.1093/nar/gkh340

607   Eren, A. M., Esen, Ö. C., Quince, C., Vineis, J. H., Morrison, H. G., Sogin, M. L., & Delmont, T. O. (2015). Anvi'o:

608   An advanced analysis and visualization platform for 'omics data. *PeerJ*, *3*, e1319.

609   https://doi.org/10.7717/peerj.1319

610   Everroad, R. C., Six, C., Partensky, F., Thomas, J.-C., Holtzendorff, J., & Wood, A. M. (2006). Biochemical Bases

611   of Type IV Chromatic Adaptation in Marine Synechococcus spp. *Journal of Bacteriology*, *188*(9), 3345–

612   3356. https://doi.org/10.1128/JB.188.9.3345-3356.2006

613   Farrant, G. K., Doré, H., Cornejo-Castillo, F. M., Partensky, F., Ratin, M., Ostrowski, M., Pitt, F. D., Wincker, P.,

614   Scanlan, D. J., Iudicone, D., Acinas, S. G., & Garczarek, L. (2016). Delineating ecologically significant

615   taxonomic units from global patterns of marine picocyanobacteria. *Proceedings of the National Academy of*

616   *Sciences*, *113*(24), E3365–E3374. https://doi.org/10.1073/pnas.1524865113

617   Grébert, T., Doré, H., Partensky, F., Farrant, G. K., Boss, E. S., Picheral, M., Guidi, L., Pesant, S., Scanlan, D. J.,

618   Wincker, P., Acinas, S. G., Kehoe, D. M., & Garczarek, L. (2018). Light color acclimation is a key process

619   in the global ocean distribution of *Synechococcus cyanobacteria*. *Proceedings of the National Academy of*

620   *Sciences*, *115*(9), E2010–E2019. https://doi.org/10.1073/pnas.1717069115

621   Holte, J., & Talley, L. (2009). A New Algorithm for Finding Mixed Layer Depths with Applications to Argo Data

622   and Subantarctic Mode Water Formation. *Journal of Atmospheric and Oceanic Technology*, *26*(9), 1920–

623   1939. https://doi.org/10.1175/2009JTECHO543.1

624   Holte, J., Talley, L. D., Gilson, J., & Roemmich, D. (2017). An Argo mixed layer climatology and database.

625   *Geophysical Research Letters*, *44*(11), 5618–5626. https://doi.org/10.1002/2017GL073426

626   Holtrop, T., Huisman, J., Stomp, M., Biersteker, L., Aerts, J., Grébert, T., Partensky, F., Garczarek, L., & Woerd, H.

627   J. van der. (2020). Vibrational modes of water predict spectral niches for photosynthesis in lakes and

628   oceans. *Nature Ecology & Evolution*. https://doi.org/10.1038/s41559-020-01330-x

629   Humily, F., Partensky, F., Six, C., Farrant, G. K., Ratin, M., Marie, D., & Garczarek, L. (2013). A Gene Island with

630   Two Possible Configurations Is Involved in Chromatic Acclimation in Marine Synechococcus. *PLoS ONE*,

631   *8*(12), e84459. https://doi.org/10.1371/journal.pone.0084459

632   Kent, A. G., Baer, S. E., Mouginot, C., Huang, J. S., Larkin, A. A., Lomas, M. W., & Martiny, A. C. (2019). Parallel

633   phylogeography of Prochlorococcus and Synechococcus. *The ISME Journal*, *13*(2), 430–441.

634   https://doi.org/10.1038/s41396-018-0287-6

635   Kumar, S., Stecher, G., & Tamura, K. (2016). MEGA7: Molecular Evolutionary Genetics Analysis Version 7.0 for

636   Bigger Datasets. *Molecular Biology and Evolution*, *33*(7), 1870–1874.

637   https://doi.org/10.1093/molbev/msw054

638   Langmead, B., & Salzberg, S. L. (2012). Fast gapped-read alignment with Bowtie 2. *Nature Methods*, *9*(4), 357–

639   359. https://doi.org/10.1038/nmeth.1923

640   Larkin, A. A., Garcia, C. A., Garcia, N., Brock, M. L., Lee, J. A., Ustick, L. J., Barbero, L., Carter, B. R., Sonnerup,

641   R. E., Talley, L., Tarran, G. A., Volkov, D. L., & Martiny, A. C. (2021). High spatial resolution global

642   ocean metagenomes from Bio-GO-SHIP repeat hydrography transects. *Scientific Data*.

643   https://doi.org/doi:10.1038/s41597-021-00889-9

644   Laske, S. M., Rosenberger, A. E., Wipfli, M. S., & Zimmerman, C. E. (2018). Generalist feeding strategies in Arctic

645   freshwater fish: A mechanism for dealing with extreme environments. *Ecology of Freshwater Fish*, *27*(3),

646   767–784. https://doi.org/10.1111/eff.12391

647   Lee, Z., Weidemann, A., Kindle, J., Arnone, R., Carder, K. L., & Davis, C. (2007). Euphotic zone depth: Its

648   derivation and implication to ocean-color remote sensing. *Journal of Geophysical Research: Oceans*,

649   *112*(C3). https://doi.org/10.1029/2006JC003802

650   Letunic, I., & Bork, P. (2007). Interactive Tree Of Life (iTOL): An online tool for phylogenetic tree display and

651   annotation. *Bioinformatics*, *23*(1), 127–128. https://doi.org/10.1093/bioinformatics/btl529

Li, H., Handsaker, B., Wysoker, A., Fennell, T., Ruan, J., Homer, N., Marth, G., Abecasis, G., Durbin, R., &
Subgroup, 1000 Genome Project Data Processing. (2009). The Sequence Alignment/Map format and
SAMtools. *Bioinformatics*, *25*(16), 2078–2079. https://doi.org/10.1093/bioinformatics/btp352

Lima, I. D. (2002). Biological response to frontal dynamics and mesoscale variability in oligotrophic environments:
Biological production and community structure. *Journal of Geophysical Research*, *107*(C8), 3111.
https://doi.org/10.1029/2000JC000393

Lovindeer, R. (2021). *CA4 model version 1.0.0* (v1.0.0) [Computer software]. Zenodo.
https://doi.org/10.5281/ZENODO.4663350

Luimstra, V. M., Verspagen, J. M. H., Xu, T., Schuurmans, J. M., & Huisman, J. (2020). Changes in water color
shift competition between phytoplankton species with contrasting light-harvesting strategies. *Ecology*,
101(3), e02951. https://doi.org/10.1002/ecy.2951

Mahadevan, A. (2016). The Impact of Submesoscale Physics on Primary Productivity of Plankton. *Annu. Rev. Mar.
Sci.*, *8*, 17.1-17.24. https://doi.org/10.1146/annurev-marine-010814-015912

Mahadevan, A., Tandon, A., & Ferrari, R. (2010). Rapid changes in mixed layer stratification driven by
submesoscale instabilities and winds. *Journal of Geophysical Research*, *115*(C3), C03017.
https://doi.org/10.1029/2008JC005203

Mahmoud, R. M., Sanfilippo, J. E., Nguyen, A. A., Strnat, J. A., Partensky, F., Garczarek, L., Abo El Kassem, N.,
Kehoe, D. M., & Schluchter, W. M. (2017). Adaptation to Blue Light in Marine Synechococcus Requires
MpeU, an Enzyme with Similarity to Phycoerythrobilin Lyase Isomerases. *Frontiers in Microbiology*, *8*.
https://doi.org/10.3389/fmicb.2017.00243

Moore, T. S., Dowell, M. D., & Franz, B. A. (2012). Detection of coccolithophore blooms in ocean color satellite
imagery: A generalized approach for use with multiple sensors. *Remote Sensing of Environment*, *117*, 249–
263. https://doi.org/10.1016/j.rse.2011.10.001

Palenik, B. (2001). Chromatic Adaptation in Marine Synechococcus Strains. *Applied and Environmental
Microbiology*, *67*(2), 991–994. https://doi.org/10.1128/AEM.67.2.991-994.2001

Picheral, M., Searson, S., Taillandier, V., Bricaud, A., Boss, E., Stemmann, L., Gorsky, G., Tara Oceans
Consortium, C., & Tara Oceans Expedition, P. (2014). *Vertical profiles of environmental parameters*

679   *measured from physical, optical and imaging sensors during Tara Oceans expedition 2009-2013* [Data set].

680   PANGAEA. https://doi.org/10.1594/PANGAEA.836321

681 Sadeghi, A., Dinter, T., Vountas, M., Taylor, B. B., Altenburg-Soppa, M., Peeken, I., & Bracher, A. (2012).

682   Improvement to the PhytoDOAS method for identification of coccolithophores using hyper-spectral

683   satellite data. *Ocean Science*, *8*(6), 1055–1070. https://doi.org/10.5194/os-8-1055-2012

684 Sager, J. C., & McFarlane, J. C. (1997). Radiation. In *Plant Growth Chamber Handbook.*

685   https://www.controlledenvironments.org/wp-content/uploads/sites/6/2017/06/Ch01.pdf

686 Sanfilippo, J. E., Garczarek, L., Partensky, F., & Kehoe, D. M. (2019). Chromatic Acclimation in Cyanobacteria: A

687   Diverse and Widespread Process for Optimizing Photosynthesis. *Annual Review of Microbiology*, *73*(1),

688   407–433. https://doi.org/10.1146/annurev-micro-020518-115738

689 Sanfilippo, J. E., Nguyen, A. A., Karty, J. A., Shukla, A., Schluchter, W. M., Garczarek, L., Partensky, F., & Kehoe,

690   D. M. (2016). Self-regulating genomic island encoding tandem regulators confers chromatic acclimation to

691   marine *Synechococcus*. *Proceedings of the National Academy of Sciences*, *113*(21), 6077–6082.

692   https://doi.org/10.1073/pnas.1600625113

693 Schlitzer, R., Anderson, R. F., Dodas, E. M., Lohan, M., Geibert, W., Tagliabue, A., Bowie, A., Jeandel, C.,

694   Maldonado, M. T., Landing, W. M., Cockwell, D., Abadie, C., Abouchami, W., Achterberg, E. P., Agather,

695   A., Aguliar-Islas, A., van Aken, H. M., Andersen, M., Archer, C., … Zurbrick, C. (2018). The

696   GEOTRACES Intermediate Data Product 2017. *Chemical Geology*, *493*, 210–223.

697   https://doi.org/10.1016/j.chemgeo.2018.05.040

698 Six, C., Thomas, J.-C., Garczarek, L., Ostrowski, M., Dufresne, A., Blot, N., Scanlan, D. J., & Partensky, F. (2007).

699   Diversity and evolution of phycobilisomes in marine Synechococcus spp.: A comparative genomics study.

700   *Genome Biology*, *8*(12), R259. https://doi.org/10.1186/gb-2007-8-12-r259

701 Sohm, J. A., Ahlgren, N. A., Thomson, Z. J., Williams, C., Moffett, J. W., Saito, M. A., Webb, E. A., & Rocap, G.

702   (2016). Co-occurring Synechococcus ecotypes occupy four major oceanic regimes defined by temperature,

703   macronutrients and iron. *The ISME Journal*, *10*(2), 333–345. https://doi.org/10.1038/ismej.2015.115

704 Stamatakis, A. (2014). RAxML version 8: A tool for phylogenetic analysis and post-analysis of large phylogenies.

705   *Bioinformatics*, *30*(9), 1312–1313. https://doi.org/10.1093/bioinformatics/btu033

706 Stomp, M., Huisman, J., de Jongh, F., Veraart, A. J., Gerla, D., Rijkeboer, M., Ibelings, B. W., Wollenzien, U. I. A.,

707 & Stal, L. J. (2004). Adaptive divergence in pigment composition promotes phytoplankton biodiversity.

708 *Nature*, *432*(7013), 104–107. https://doi.org/10.1038/nature03044

709 Stomp, M., Huisman, J., Vörös, L., Pick, F. R., Laamanen, M., Haverkamp, T., & Stal, L. J. (2007). Colourful

710 coexistence of red and green picocyanobacteria in lakes and seas. *Ecology Letters*, *10*(4), 290–298.

711 https://doi.org/10.1111/j.1461-0248.2007.01026.x

712 Stomp, M., van Dijk, M. A., van Overzee, H. M. J., Wortel, M. T., Sigon, C. A. M., Egas, M., Hoogveld, H., Gons,

713 H. J., & Huisman, J. (2008). The Timescale of Phenotypic Plasticity and Its Impact on Competition in

714 Fluctuating Environments. *The American Naturalist*, *172*(5), E169–E185. https://doi.org/10.1086/591680

715 Sun, C., Zhang, L., & Yan, X. (2011). Stream-coordinate structure of oceanic jets based on merged altimeter data.

716 *Chinese Journal of Oceanology and Limnology*, *29*(1), 1–9. https://doi.org/10.1007/s00343-011-9938-4

717 Sunagawa, S., Coelho, L. P., Chaffron, S., Kultima, J. R., Labadie, K., Salazar, G., Djahanschiri, B., Zeller, G.,

718 Mende, D. R., Alberti, A., Cornejo-Castillo, F. M., Costea, P. I., Cruaud, C., d'Ovidio, F., Engelen, S.,

719 Ferrera, I., Gasol, J. M., Guidi, L., Hildebrand, F., … Bork, P. (2015). Structure and function of the global

720 ocean microbiome. *Science*, *348*(6237). https://doi.org/10.1126/science.1261359

721 Taylor, J. R., & Ferrari, R. (2011). Ocean fronts trigger high latitude phytoplankton blooms. *Geophysical Research*

722 *Letters*, *38*(23). https://doi.org/10.1029/2011GL049312

723 Tilstone, G. H., Míguez, B. M., Figueiras, F. G., & Fermín, E. G. (2000). Diatom dynamics in a coastal ecosystem

724 affected by upwelling: Coupling between species succession, circulation and biogeochemical processes.

725 *Marine Ecology Progress Series*, *205*, 23–41. https://doi.org/10.3354/meps205023

726 Ustick, L. (2021). *Metagenome Cluster Coverage*. Zenodo. https://doi.org/10.5281/zenodo.4677447

727 van Dongen, S., & Abreu-Goodger, C. (2012). Using MCL to Extract Clusters from Networks. *Bacterial Molecular*

728 *Networks*, 281–295. https://doi.org/10.1007/978-1-61779-361-5_15

729 Viol, I. L., Jiguet, F., Brotons, L., Herrando, S., Lindström, Å., Pearce-Higgins, J. W., Reif, J., Turnhout, C. V., &

730 Devictor, V. (2012). More and more generalists: Two decades of changes in the European avifauna.

731 *Biology Letters*. https://doi.org/10.1098/rsbl.2012.0496

732   Walworth, N. G., Zakem, E. J., Dunne, J. P., Collins, S., & Levine, N. M. (2020). Microbial evolutionary strategies

733   in a dynamic ocean. *Proceedings of the National Academy of Sciences*, *117*(11), 5943–5948.

734   https://doi.org/10.1073/pnas.1919332117

735   Xia, X., Liu, H., Choi, D., & Noh, J. H. (2018). Variation of Synechococcus Pigment Genetic Diversity Along Two

736   Turbidity Gradients in the China Seas. *Microbial Ecology*, *75*(1), 10–21. https://doi.org/10.1007/s00248-

737   017-1021-z

738   Zwirglmaier, K., Jardillier, L., Ostrowski, M., Mazard, S., Garczarek, L., Vaulot, D., Not, F., Massana, R., Ulloa,

739   O., & Scanlan, D. J. (2008). Global phylogeography of marine Synechococcus and Prochlorococcus reveals

740   a distinct partitioning of lineages among oceanic biomes. *Environmental Microbiology*, *10*(1), 147–161.

741   https://doi.org/10.1111/j.1462-2920.2007.01440.x

742
743